EPSL

Quantification of magnetic coercivity components by the analysis of acquisition curves of isothermal remanent magnetisation

Pauline P. Kruiver *, Mark J. Dekkers, David Heslop

Paleomagnetic Laboratory 'Fort Hoofddijk', Budapestlaan 17, 3584 CD Utrecht, The Netherlands

Abstract

A new method of analysing isothermal remanent magnetisation (IRM) acquisition curves based on cumulative log Gaussian analysis [Robertson and France, Phys. Earth Planet. Inter. 82 (1994) 223–234] is proposed. It is based on the curve fitting of the IRM acquisition curve versus the logarithm of the applied field with: (i) the acquisition curve on a linear scale, (ii) the acquisition curve expressed as a gradient, and (iii) the acquisition curve on a probability scale. Even when a sample is not saturated, its magnetic properties can be defined, although with less certainty. The number of magnetic components required for an optimal fit to a measured IRM acquisition curve is evaluated statistically. The method discriminates on the basis of different mineral coercivity. Therefore, additional rock-magnetic tests are still required to separate minerals with similar coercivities. © 2001 Elsevier Science B.V. All rights reserved.

Keywords: coercivity; isothermal remanent magnetization; magnetic minerals; magnetic properties

1. Introduction

Over the last few decades rock magnetism has proven to be very useful in distinguishing magnetic minerals in various rocks, in particular at very low concentrations. Such rock-magnetic investigations aim to provide information concerning the origin of magnetic minerals, which is required for a proper palaeomagnetic interpretation of natural remanent magnetisation components. Also, rock-magnetic concepts and techniques are increasingly applied in environmental magnetism. Subtle changes in the sedimentary environment can be detected and explained in terms of factors such as varying degrees of weathering, often related to climate changes, or a varying provenance area.

One of the more commonly applied measurement types is the determination of acquisition curves of the isothermal remanent magnetisation (IRM). These data are comparatively easy to obtain. Usually, only saturation IRM (SIRM) is measured for a set of samples; the remanent coercive force is determined less often. In cases of mixed magnetic mineralogy, the contributions of individual magnetic minerals add linearly to yield a cumulative curve, provided magnetic grain in-

------

* Corresponding author. Tel.: +31-30-253-1672;
Fax: +31-30-253-1677; E-mail: kruiver@geo.uu.nl

teraction is negligible. Extraction of individual contributions from a measured curve has been attempted for a long period. Carmichael [2] inferred a hard and a soft component from the shape of a backfield IRM curve, however, without explicitly explaining how the separation was achieved. Because the low-field part of an IRM acquisition curve of magnetically hard material is approximately linear, Dekkers [3] extrapolated linearly back to the ordinate axis to separate soft and hard components. However, establishing an appropriate point from where to extrapolate appeared to be problematic in a number of cases. Robertson and France [1] observed experimentally that the IRM acquisition curves of individual minerals conform to a cumulative log-Gaussian (CLG) curve. A measured IRM curve can therefore be decomposed into a number of CLG curves, which can be individually characterised by their SIRM, mean coercivity and dispersion. IRM curve fitting has been applied earlier based on the gradient of the curve [4]. Stockhausen [5] provided three parameters to access the goodness of fit for the log-Gaussian components. However, no criteria were given to indicate when each parameter should be used. In this paper we present a new method to determine magnetic coercivity distributions, which is based on the CLG appearance of IRM acquisition curves [1]. We will demonstrate that it is possible to quantify a magnetic distribution, even when it is far from being saturated.

2. Cumulative log-Gaussian analysis

Robertson and France [1] showed that the IRM acquired by natural magnetic assemblages can be approximated by a CLG function of the magnetising field (Fig. 1a). This is because the magnetic grain-size distribution is logarithmic, typical of trace constituents in rocks. If no magnetic interactions occur, an assemblage of grains of a single magnetic mineral can be characterised by: (i) its SIRM, (ii) the field at which half of the SIRM is reached: $B_{1/2}$ (or B_{cr}') and (iii) the width of the distribution: the dispersion parameter DP, given by one standard deviation of the logarithmic distribution (Fig. 1). If more than one magnetic mineral is present, their IRM acquisition curves add linearly (Fig. 2a). The effects of small deviations from a log-normal distribution will be discussed by Heslop (in preparation).

Based on the assumption that an IRM acquisition curve follows a CLG function, we perform two transformations: (i) field values are converted to their logarithmic values and (ii) the linear ordinate scale is converted to a probability scale. This is done by standardising the acquisition curve. After these transformations, a unimodal distribution is represented by a straight line (Fig. 1c). The squares are an example of a natural sample of a single magnetic mineral (titanomagnetite) and as such the data plot as a straight line. Plotting an IRM acquisition curve in this way is visually appealing: it is immediately obvious when the
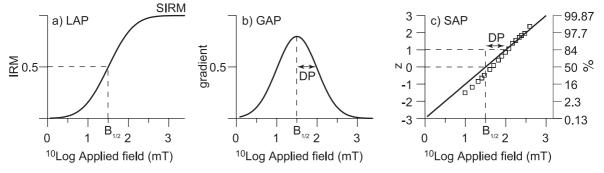

Fig. 1. (a) An example of an IRM acquisition curve, called the linear acquisition plot (LAP). (b) The gradient of acquisition plot (GAP). The dispersion parameter (DP) represents one standard deviation. (c) The IRM acquisition curve on a probability scale (right-hand ordinate) and corresponding z-score scale (left-hand ordinate), called the standardised acquisition plot (SAP). Solid line (including DP and $B_{1/2}$) is for the IRM acquisition curve shown in panel a. Squares are measured data from a single magnetic mineral sample (titanomagnetite). Note that the abscissa is logarithmic for all three plots.
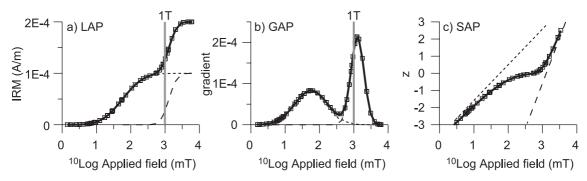
Fig. 2. (a) LAP for a modelled mixture of magnetite (SIRM = 0.1 mA/m, $\log(B_{1/2})$ = 1.76, DP = 0.48) and goethite (SIRM = 0.1 mA/m, $\log(B_{1/2})$ = 3.11, DP = 0.19). Squares represent synthetic data. Short-dashed line represents component 1; long-dashed line component 2. Solid line represents the sum of the components. 1 T cut-off point is indicated for the study of the effect of non-saturation. (b) GAP analysis for the modelled mixture. Lines and symbols as in panel a. (c) SAP analysis for the modelled mixture. Lines and symbols as in panel a.

IRM acquisition curve needs to be fitted with more than one component, because the data points do not plot on a linear path. For convenience, the non-equidistant cumulative percentage scale is replaced by the equivalent equidistant standardised z-scores [6] which are easier to plot. Fifty per cent of the cumulative distribution corresponds to a standardised value of $z = 0$ at field $B_{1/2}$; 84.1% (one standard deviation from the centre) corresponds to $z = 1$ at field $B_{1/2}$+DP, etc. Note that $|z| > 3$ represents only $2 \times 0.13\%$ of the distribution. The analysis of IRM acquisition curves on a linear ordinate scale is referred to as LAP (linear acquisition plot); as a gradient curve as GAP (gradient of acquisition plot); and on a probability scale as SAP (standardised acquisition plot). The combined analysis

of LAP, GAP and SAP is referred to as CLG analysis.

The three different representations from the IRM data are plotted in an Excel workbook. Curve fitting is performed by forward modelling. Initial values for SIRM, $\log(B_{1/2})$ and DP are estimated from the LAP, GAP and SAP. These values are entered in the program and for the specified distributions the theoretical IRM curves are calculated and added. The modelled LAP, GAP and SAP are compared to the data. The goodness of fit is expressed by the sum of the squared differences between the data and the model (squared residuals) for each plot. The values for SIRM, $\log(B_{1/2})$ and DP are optimised interactively by minimising these squared residuals. Before showing some examples illustrating

Table 1
The effect of data truncation for a modelled mixture of magnetite and goethite (Fig. 2) to a maximum applied field of 1 T, as well as the effect of addition of various levels of normally distributed random noise (as ± a percentage of the total SIRM)

	Component 1			Component 2				Squared residuals		
	SIRM (mA/m)	$\log(B_{1/2})$	DP	SIRM (mA/m)	$\log(B_{1/2})$	DP	n	LAP	GAP	SAP
Input	0.100	1.76	0.48	0.100	3.11	0.19	53			
Recovered	0.100	1.76	0.48	0.100	3.11	0.19	53	6.08e−12	6.05e−11	7.54e−3
Truncated	0.101	1.76	0.48	0.100	3.11	0.19	41	2.44e−11	4.13e−11	2.22e−3
0% noise	0.100	1.76	0.48	0.101	3.11	0.19	44	1.41e−11	7.12e−11	1.28e−3
1% noise	0.100	1.77	0.51	0.100	3.11	0.19	44	5.69e−11	3.41e−7	1.46e−1
2% noise	0.100	1.77	0.53	0.100	3.11	0.19	44	1.82e−10	1.36e−6	4.51e−1
3% noise	0.100	1.78	0.54	0.100	3.11	0.17	44	4.47e−10	3.04e−6	8.99e−1

n is the number of data points included in the analysis. Squared residuals are summed squared differences between the modelled total IRM curves and the measured data.

the merit of the approach we address three aspects of the CLG technique: (i) the effect of non-saturation, (ii) the effect of noise in the data and (iii) the statistics for the optimal fit.

2.1. The effect of non-saturation

Because many laboratories have IRM facilities which reach up to ca. 1 T, it is necessary to investigate how non-saturated IRM acquisition curves behave in the CLG analysis. To study the effect of saturation of the IRM, we modelled a mixture of magnetite and goethite (Fig. 2). For the purpose of clarity, we chose two minerals with very different coercivities. However, the method works equally well with components with (partly) overlapping coercivity components. With large overlaps, however, more data points are required for a statistically meaningful separation. When the mixture is fully saturated, the two distributions appear as two Gaussian curves in a GAP and as two linear segments in a SAP (Fig. 2b,c). The input parameters can be accurately reproduced (Table 1). For the analysis in Fig. 3, the IRM acquisition curve has been truncated at 1 T, corresponding to 64% saturation. Non-saturation shows up as a partially visible Gaussian curve in the GAP analysis and as a concave curve in the SAP analysis. This 'curl' at higher fields is indicative of non-saturation (Fig. 3b). Although only

part of the high-field component is defined by the data, again the input parameters are faithfully reproduced (Table 1). The level of saturation can be estimated from the measured maximum IRM and the sum of the modelled SIRM values.

2.2. The effect of noise

To study the stability of the method described, we added several levels of normally distributed random noise to the synthetic curve of Fig. 2 to mimic the effect of measurement noise inherent to the data acquisition. We assessed the noise levels found in a real data sample (Fig. 6) by comparing the values of the squared residual array produced during the modelling procedure to the measured IRM data. From this investigation it appeared that the difference between the modelled IRM and the measured IRM data is typically in the order of ± 1–2% of the total SIRM. Therefore, we scaled the random noise array to ± 1, 2 and 3% (of the total SIRM) and combined it with the modelled IRM data before re-evaluating the best-fit parameters of the individual IRM components (Table 1, ± 0–3% noise). After the addition of the noise array to the IRM curve a number of points had to be removed from the input data set (e.g. negative IRM intensities at low fields). This resulted in a total of 44 acquisition points that could be used in the fitting procedure.
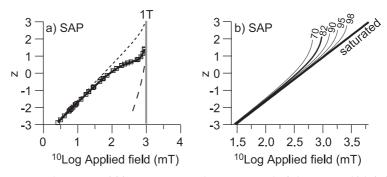

Fig. 3. (a) SAP analysis for the truncated IRM acquisition curve. Note the concave end of the curve, which is indicative of non-saturation. Lines and symbols as in Fig. 2. (b) The effect of non-saturation on the SAP, modelled for a haematite with $\log(B_{1/2}) = 2.64$ ($B_{1/2} = 437$ mT) and DP = 0.39. Numbers indicate the level of saturation. In this example, 82% corresponds to a maximum applied field of 1 T.

Table 2
Coercivity values for three samples taken from a hydromorphous soil layer and one sample from a caliche bed

Sample	Comp.	SIRM (A/m)	$\log(B_{1/2})$ (mT)	$B_{1/2}$	DP	Contr. (%)
Hydromorphous soil bed						
GLO108	1	0.23	1.90	79 mT	0.45	33
Fit 1	2	0.47	3.70	5.0 T	0.50	67
GLO108	1	0.23	1.90	79 mT	0.45	28
Fit 2	2	0.60	3.80	6.3 T	0.50	72
GLO108	1	0.18	1.75	56 mT	0.35	28
Fit 3	2	0.019	2.16	145 mT	0.13	3
	3	0.44	3.60	4.0 T	0.60	69
GLO113	1	0.10	1.65	45 mT	0.38	9
	2	1.06	3.30	2.0 T	0.29	91
GLO117	1	0.062	1.70	50 mT	0.46	33
	2	0.124	3.25	1.8 T	0.28	67
Caliche bed						
GLO100	1	0.55	1.56	36 mT	0.37	14
	2	3.44	2.62	417 mT	0.44	86

For sample GLO108 three possible interpretations are given.

As expected, the deviation of the model fit from the input values increases for increasing noise levels, resulting in larger squared residuals. Particularly, the GAP squared residuals increase because a gradient is considered. For ±1 and 2% noise, the components are recovered well: randomly distributed noise only yields slightly larger DPs for component 1 and a small shift in $\log(B_{1/2})$, for component 2 the effect is too small to be noticed. It should be realised that noise scaling to the total IRM represents a 'worst-case scenario': for real data, each data point has a measurement noise of ∼2%. The scaling to total IRM also induces a seemingly larger noise level in component 1 than in component 2. Therefore, it exerts a greater influence over the smaller IRM values in the low-coercivity portion of the acquisition curve. This analysis shows that for realistic levels of normally distributed random noise the input IRM components can be reproduced within acceptable limits.

2.3. Statistics

The merit of the statistics is twofold. It can be used: (i) to determine whether the addition of an extra component significantly improves the fit and (ii) to investigate the range of possible values for the chosen components, i.e. when two fits are equally good from a statistical viewpoint, information on the variability of the components is obtained. The sums of the squared residuals are used as proxies for the goodness of fit. First, an *F*-
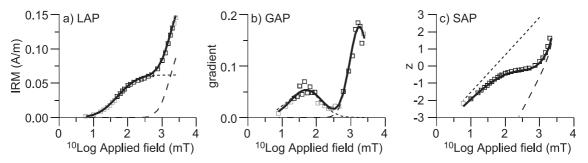

Fig. 4. (a) LAP, (b) GAP and (c) SAP for a real data example of a hydromorphous soil sample (GLO117, Table 2). Lines and symbols as in Fig. 2.

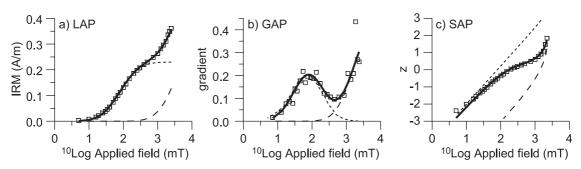*P.P. Kruiver et al. / Earth and Planetary Science Letters 189 (2001) 269–276*

Fig. 5. (a) LAP, (b) GAP and (c) SAP of fit 1 for a real data example of hydromorphous soil sample (GLO108, Table 2). Lines and symbols as in Fig. 2. Fit 2 looks very similar, fit 3 allows for an extra component in the low coercivity range.

test is applied in order to determine whether the variance of the squared residuals for one interpretation is significantly smaller than the variance of the other interpretation (with a specified level of significance, α) [6]. If so, the best fit is represented by the parameter values which result in the smallest variance of squared residuals. If the variances are statistically indistinguishable on an α level, a Student's t-test is applied in order to determine whether the average squared residual of one interpretation is significantly smaller than the average squared residual of the other interpretation [6]. If so, the parameter values which result in the smallest average squared residual represents the best fit. If the average squared residuals are statistically indistinguishable, the interpretations are equally good. In these cases, other criteria, like similarity to other samples in the data set, should be used along with the statistics to decide which interpretation is best. It should be noted, however, that the statistics are not always conclusive for the LAP, GAP and SAP at the same time.

3. Some examples

Examples of natural mixtures which cannot be saturated in fields of 2.5 T are found in a hydromorphous soil layer in the continental red bed section of La Gloria in central Spain [7]. In general, the section contains haematite and variably oxidised magnetite. The hydromorphous soil layer, however, has the yellow appearance indicative of goethite. Three samples of this layer are analysed (GLO108, GLO113 and GLO117 in Ta-

ble 2, Figs. 4 and 5). In all three samples, the second component is only partially defined. Still, it can be characterised within narrow limits (on a logarithmic scale). Component 1 is interpreted as oxidised magnetite and component 2 as goethite (confirmed by thermal demagnetisation). The differences in $B_{1/2}$ and DP values for component 1 are interpreted as varying degrees of oxidation of the magnetite. Differences in coercivity of component 2 in the three samples can be explained by changes in crystallinity of the goethite or by variable substitution [8].

The test statistics are applied to three possible interpretations (fits 1–3) for sample 108, which was hardest to analyse. Fig. 5 shows LAP, GAP and SAP for fit 1. The curves are very similar for

Table 3
F-test and t-test results for the three interpretations of GLO108

		F-test	t-test	Test results
Fit 1 and Fit 2	LAP	4.99		Fit 1 better
	GAP	1.38	0.02	no difference
	SAP	1.01	0.02	no difference
Fit 1 and Fit 3	LAP	14.4		Fit 1 better
	GAP	1.25	0.23	no difference
	SAP	14.3		Fit 1 better
Fit 2 and Fit 3	LAP	2.89		Fit 2 better
	GAP	1.72	0.21	no difference
	SAP	14.5		Fit 2 better

For 27 data points and a confidence level of 95%, the critical F value is 1.88. Below this value the variance for one fit is not significantly smaller than for the other. The critical t value is 1.68. Below this value the average squared residual for one fit is not significantly smaller than for the other. Only when the F value is below the critical F, the t-test may be applied.
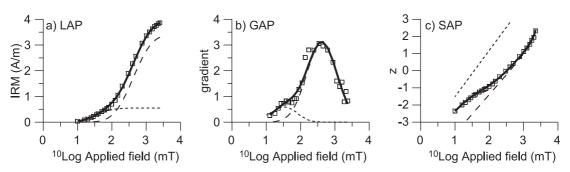
Fig. 6. (a) LAP, (b) GAP and (c) SAP for a real data example of a caliche red bed sample (GLO100, Table 2). Lines and symbols as in Fig. 2.

the three interpretations. The decision on the best fit could not be made by eye. The results of the F-tests and t-tests at a 95% confidence level are given in Table 3. According to the gradient plot, one could choose to fit two or three components. From the comparison of fits 1 and 3, and of fits 2 and 3 we conclude that fit 3 is worse than fit 1 and fit 2. The seemingly present third component in the gradient plot is due to data scatter. Therefore, the two-component fit is to be favoured over the three-component fit. However, the tests are not conclusive between fits 1 and 2, so these interpretations are equally good from a statistical viewpoint. Thus, the coercivity of the goethite ranges from 5.0 to 6.3 T. Also note that the 'curl' in Fig. 5c is more prominent than in Fig. 4c. This is explained by the higher coercivity of the goethite in sample GLO108, which is thus less saturated by a 2.5 T field.

An example of a mixture of two partly overlapping coercivities is taken from a caliche bed located approximately 1 m below the hydromorphous soil layer. This sample is representative of the red beds in this section (Fig. 6, Table 2). The first component is interpreted as a slightly oxidised magnetite. It is less oxidised than the magnetite in the hydromorphous soil, because both $B_{1/2}$ and DP are lower. The second component is interpreted as haematite with a $B_{1/2}$ of ~ 417 mT.

4. Discussion and conclusions

In order to obtain a satisfactory fit, the IRM acquisition curve should consist of at least 25 data points. Additionally, field values should be approximately equally spaced on a logarithmic scale. During the calculation of the SAP, remanence values are normalised to the maximum IRM value. Therefore, this data point does not appear in the SAP. Hence, it is advised to take the two highest field measurements at values which are close together.

It should be emphasised that the most consistent interpretation is obtained by combining the LAP, GAP and SAP analyses. SAP analysis only provides relative contributions of the components, because of the normalisation of the IRM curve. The IRM acquisition curve and the gradient analysis provide the absolute SIRMs. However, the gradient method is sensitive to data errors, because it uses a derivative. Therefore, data scatter in the gradient plot is larger. Subtle changes in coercivities are easily overlooked in the LAP. With the combination of the three plots, it is possible to obtain a robust determination of the components. Initial SIRM values can be easily estimated from the LAP; the GAP provides initial values for $\log(B_{1/2})$ and DP. The fit is then interactively optimised by minimising the squared residuals for the three representations of the curve. In studying the magnetic properties and by the curve-fitting, one is forced to consider possible source areas and processes which led to the measured IRM acquisition curve. In this quantitative manner, considerably more information can be obtained from the same measured curve. A computer program (Excel workbook) including a manual is provided via internet

(www.geo.uu.nl/∼forth/; follow the link for 'Publications').

With increasing coercivity overlap, it evidently will become harder to distinguish components. Automated IRM data acquisition enabling gathering of many data points is available in some instruments and should be used advantageously. For magnetic minerals with similar coercivities (e.g. magnetite and greigite and to a lesser extent pyrrhotite, or haematite and some goethites) additional rock-magnetic tests could be required, for example thermal demagnetisation or low-temperature cycling. CLG analysis as proposed here can then be used as a tool to select suitable peak fields for orthogonal IRM thermal demagnetisation [9].

Acknowledgements

References

[1] D.J. Robertson, D.E. France, Discrimination of remanence-carrying minerals in mixtures, using isothermal remanent magnetisation acquisition curves, Phys. Earth Planet. Inter. 82 (1994) 223–234.

[2] C.M. Carmichael, The magnetic properties of ilmenite-haematite crystals, Proc. R. Soc. A 263 (1961) 508–530.

[3] M.J. Dekkers, Magnetic properties of natural goethite. III. Magnetic behaviour and properties of minerals originating from goethite dehydration during thermal demagnetization, Geophys. J. Int. 103 (1990) 233–250.

[4] D.N. Thomas, T.C. Rolph, D.F. Friel, Permo-Carboniferous (Kiaman) palaeointensity results from the western Bohemian Massif, Germany, Geophys. J. Int. 130 (1997) 257–265.

[5] H. Stockhausen, Some new aspects for the modelling of isothermal remanent magnetization acquisition curves by cumulative log Gaussian functions, Geophys. Res. Lett. 25 (1998) 2217–2220.

[6] A.R.H. Swan, M. Sandilands, Introduction to Geological Data Analysis, Blackwell Science, Oxford, 1995, 446 pp.

[7] W. Krijgsman, M. Garcés, C.G. Langereis, R. Daams, J. van Dam, A.J. van der Meulen, J. Agustí, L. Cabrera, A new chronology for the middle to late Miocene continental record in Spain, Earth Planet. Sci. Lett. 142 (1996) 367–380.

[8] M.J. Dekkers, Magnetic properties of natural goethite. I. Grain size dependence of some low- and high-field related rockmagnetic parameters measured at room temperature, Geophys. J. 97 (1989) 323–340.

[9] W. Lowrie, Identification of ferromagnetic minerals in a rock by coercivity and unblocking temperature properties, Geophys. Res. Lett. 17 (1990) 159–162.